Simulation and Experimental Analysis of Electrical Characterization of Cap-Pin Glass Insulator under Uniform and Non-Uniform Pollution Layers

Rabie Salhi[1*], Abdelouahab Mekhaldi[1], Madjid Teguar[1], Omar Kherif[2]

[1] Laboratoire de Recherche en Electrotechnique (LRE), Ecole Nationale Polytechnique (ENP), 16200 El Harrach, Algiers, P.O.B. 182, Algeria
[2] Advanced High Voltage Engineering Research Centre, School of Engineering, Cardiff University, Queen's Buildings, 14–17 The Parade, CF24 3AA Cardiff, United Kingdom
* Corresponding author, e-mail: rabie.salhi@g.enp.edu.dz

Abstract

This paper deals with the analysis of the electrical performance of the glass cap-pin insulator under pollution conditions. The experiments are conducted in accordance with the IEC TS 60815-1:2008 standard using artificial pollution (a distilled water mixture with NaCl). Several levels of applied voltage are used to evaluate the impact of both uniform and non-uniform pollution. For the same conditions, simulations are carried out using the COMSOL Multiphysics environment. Of interest, Leakage current waveforms are extracted from the current density and compared to those obtained from experiments. A proposed process, which aims to predict the effectiveness of the simulation in selecting appropriate parameters, geometry, boundaries etc., is investigated, where the findings are closely match the real model. Therefore, the electric field distribution on the insulator surface is presented, and 3D representations are considered for better visualizing the influence of the pollution on the insulating system. Accordingly, arcing discharges are characterized by high levels of electric field stress for uniform pollution, and dry-band arcing is simulated to correspond perfectly with laboratory findings for non-uniform pollution. Finally, this paper provides valuable insights into the electrical stress on the insulator under the effect of pollution conditions.

Keywords

cap-pin insulator, COMSOL, leakage current, electric field, arcing discharges

1 Introduction

In the face of its ever-increasing demand, the electric power is transported over long distances mainly by a large electrical system mainly including overhead transmission lines. Taking into account the lack of storage for this energy and reducing power line losses [1], boosting the voltage level is one of the proposed alternatives, considering its techno-economic aspect [2]. This increase results in an improvement in the insulators, which are key components in overhead lines, HVAC, and HVDC [3, 4]. Consequently, several studies (e.g., [5, 6]) have been carried out to improve the efficiency of these components. Most of these studies were based on the computation of electric potential and the improvement of the distribution of the electric field. This latter is assumed to be an important and decisive feature in insulating design since it widely affects the HV insulators behavior [7].

In fact, the electric field can be strengthened in the presence of pollution on insulators surfaces, including wetted solid pollutant particles such as dust and sand, salt-fog, moisture, haze, and more [1]. These contaminants form a conducting layer on the insulator surface, allowing leakage current to flow through it. This can result in the occurrence of the arcing and even flashovers [6], leading to a reduction in the insulator's performance [8] and potentially causing power outages [4]. To prevent such situations, monitoring of insulators surfaces is necessary. For this, various methods using air pollution sensors and optical system detectors, or basing on surface conductance and/or leakage current measurements have been employed to predict the severity of contamination on HV insulators [9]. New technologies based on aerial images taken by drones are also cost-effective on hard ground or in severe weather conditions [10].

Studying LC on the insulators for HV transmission lines has shown an increased interest [3, 11]. Therefore, various techniques have been developed to analyze LC waveforms in order to further contribute to the explanation of discharge activities and flashover process stages [9, 12]. Some authors have employed off-line LC measurements methods. For instance, the detection of LC using the electromagnetic field was reported in [13].

On-line LC measurements have a big advantage in preventing insulator failure. Therefore, in [3], researchers developed a real-time wireless device for monitoring HVAC insulators. Similarly, measuring instruments were installed on HVDC where glass and composite insulators were both installed on the V-line to investigate LC [14].

In addition, since they help in making decisions and predictions. Using suitable numerical software, some researchers have determined and investigated LC waveforms on insulators under pollution. An equivalent circuit of a glass insulator was presented in [15] using ATPDraw software. The simulated results were very close to those obtained by experiments. In [16], researchers established a dynamic improved model to analyze LCs on polluted insulators.

Simulation techniques are also effective in investigating the electrical performance of insulators. They have been used to optimize the electric field intensity, i.e., insulator performance, by targeting insulator dimensions [17] or corona ring design [18]. Simulation has also been utilized in [19] to evaluate the residual resistance of the surface insulator pollution layer. The effect of pollution on cap-pin glass insulators' PD activities has been examined in [20] using both simulation and experimental studies, suggesting that PD activities are concentrated in areas where the electric field is reinforced. In general, selecting simulation parameters is crucial for modelling real-world scenarios. For instance, to validate simulation results, researchers in [21] have proposed an experimental technique for measuring surface voltage along insulator strings. Leakage current is also a suitable subject to predict the effectiveness of the simulation in selecting appropriate parameters, geometry, and boundaries to closely match the real model, this approach which not considered in previous researches, is proposed in this study.

This paper presents a computational approach under COMSOL Multiphysics environment, alongside laboratory experiments, to investigate cap-pin glass insulators subjected to both uniform and non-uniform pollution conditions. The main objective of this study is to analyze leakage current (LC) waveforms at different levels of applied voltage and pollution severities. A comparative analysis of simulated and experimental LC waveforms and magnitudes is also presented, providing the level of similarity between the real insulator and simulated model. Further information about the LC is given through the simulation and investigation of current density streamlines. As a valid complement to experimental tests, the simulation allows obtaining the 3D representation of the electric field distribution on the insulator under both pollution conditions, and then identifying areas with arcing activity characterizing by high electric field intensities. It is worth noting that the LC waveforms, as well as the areas of the arcing activity extracted by simulation, have never been done so far.

2 Experimental setup

Section 2 covers the experimental procedure employed to analyze the behavior of the HV insulator under pollution. This insulator, commonly called 1512L glass cap-pin, is widely used in Algerian HV transmission lines strings. This insulator has a maximum diameter of $D = 254$ mm, a height of $H = 146$ mm, and a leakage path of $L = 292$ mm (Fig. 1).

The tests were conducted at the HV laboratory of Ecole Nationale Polytechnique (ENP) in Algiers. The procedure consisted of measuring the LC on the insulator under both uniform and non-uniform pollution conditions, in accordance with the IEC TS 60815-1:2008 standard [22]. To assess the level of pollution severity, tests were also conducted on a clean insulator, which was used as a reference.

The experimental setup used in this study consists of a HV test transformer (300 kV, 50 kVA, 50 Hz) supplied by a regulating transformer (0 to 380 V, 50 kVA, 50 Hz) and a filter placed between them (Fig. 2). The applied voltage is measured using an AC capacitive voltage divider with a ratio of 1:1000 ($C_1 = 500$ pF and $C_2 = 0.5$ μF). LC is measured by recording the voltages across a measuring resistor
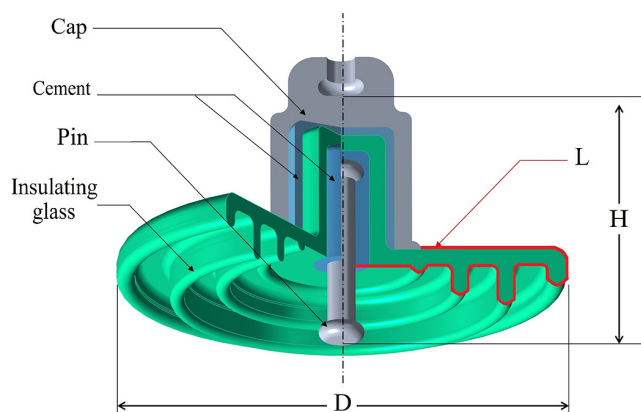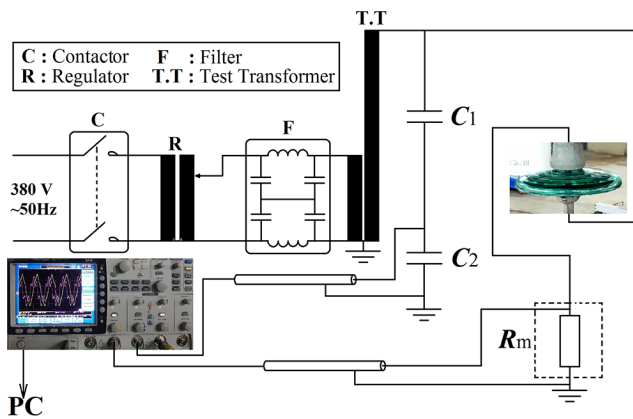

Fig. 1 Cap-pin insulator

Fig. 2 Schematic diagram of the experimental setup

R_m inserted in series with the test insulator. The resistor values used to measure LC for uniform and non-uniform pollution conditions are 100 Ω and 1 kΩ, respectively. To avoid undesirable signals, each resistor was enclosed in a grounded metallic cover forming a Faraday cage.

LC and voltage waveforms are transmitted via coaxial cables to a digital oscilloscope for visualization and recording. The INSTEK GDS-3504 with a bandwidth of 500 MHz was used for this purpose. A computer was employed to record the applied voltage and LC waveforms on the polluted insulator.

The experiment was conducted for clean, uniform, and non-uniform surface pollution. To ensure the cleanliness of the insulator, most impurities were eliminated from the surface [8, 9]. For this, the insulator surface was washed with water and dried using paper. It was then cleaned using cotton with pure alcohol (99.8%) and left to dry naturally. The artificial pollution considered in this investigation mainly consists of distilled water and NaCl. Several masses of NaCl (i.e., various concentrations) were adopted to reproduce different levels of site pollution severity (SPS) classes (from very light to medium) as stated in the IEC TS 60815-1:2008 standard [22]. The corresponding pollutant solutions were prepared in ENP's HV laboratory, and their conductivity values are listed in Table 1 according to the NaCl quantities used in 1 L of distilled water.

To apply the artificial layer pollution onto the insulator surface, the prepared pollutant solution was sprayed using a sprayer. In order to keep the same reproductibility of the solution pollution, we have chosen 6 sides, spaced

Table 1 Solution conductivity

	Very light	Light	Medium
Mass of NaCl [mg]	0	100	250
Conductivity [µS/cm]	20	150	340

at 60 degrees, forming a circle. This solution was sprayed three times on each side. The distance between the spray nozzle and the insulator surface has been kept at 40 cm from the insulator. Such experimental procedure was used on the top and bottom of the insulator (Fig. 3) according to the IEC 60507:2013 [23].

As mentioned previously, uniform and non-uniform pollution distributions were considered. For the uniform distribution, the pollutant solution was spread uniformly all over the insulator surface (upper and lower parts). For non-uniform pollution distribution, starting from the HV side, we adopted several pollution layer widths of 5, 10, 15, 20, and 25 cm. To avoid weighing down the paper, we present for this (non-uniform pollution) distribution the results corresponding to the very heavy pollution severity, in which the conductivity value of the contaminant solution is 1050 µS/cm for mass of NaCl of 750 mg.

In order to fixate the pollution on the insulator surface with varying layer widths of 5, 10, 15, 20, and 25 cm, we employed absorbent paper strips matching each layer's width precisely. We then filled these strips with the pollution solution. This is mainly to ensure a uniform distribution of the pollution solution across the designated layer with the selected widths, preventing its spread onto the dry band surface.

3 Simulation procedure

We conducted simulations using the Electric Current Module of COMSOL Multiphysics; FEM-based software for solving PDE equations. The same pollution conditions cited previously were applied to the cap-pin insulator design.

The insulator pin is energized using the same time-dependent applied voltage ($V(t)$) as in the laboratory, under
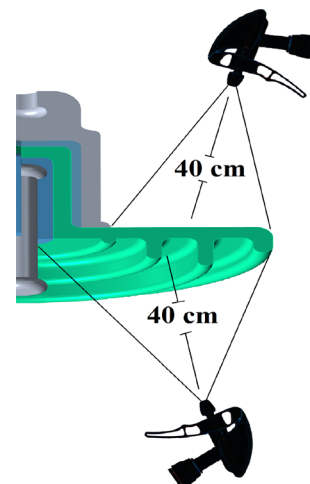

Fig. 3 Spraying sides method

50 Hz, while the cap is grounded. The air is modelled as a circle with a radius of 2 m, and its external boundary is electrically insulated ($\boldsymbol{n} \times \boldsymbol{J} = 0$). It is worth mentioning that an extremely fine free triangular mesh was used to obtain better mesh quality, particularly for the corners and small rounded edges.

After solving the problem and finding the solutions related to potential and electric field distributions, we focused on the extraction of LC waveforms based on the concept of the surface integral of the current density. This technique was explicitly explained in a previous study [24], in which all material parameters considered in this study are presented in Table 2. Furthermore, the relative permittivity value of the pollution was set to 80.

In order to extract the total LC waveform, firstly, we used the surface integral through an area where the normal current density is directed. Therefore, it is crucial to apply uniformly the potential on a volume fully enclosed by the surface (S), which includes the cap and pin electrodes.

The second stage is related to the pollution layer thickness. In the case of non-uniform pollution (Fig. 4 (a) to (e)), this thickness has been chosen as 1 mm (it can be between 1 and 2 mm [20]). For the uniform pollution (Fig. 4 (f)), we determined the thickness (e_p) of the uniform pollution
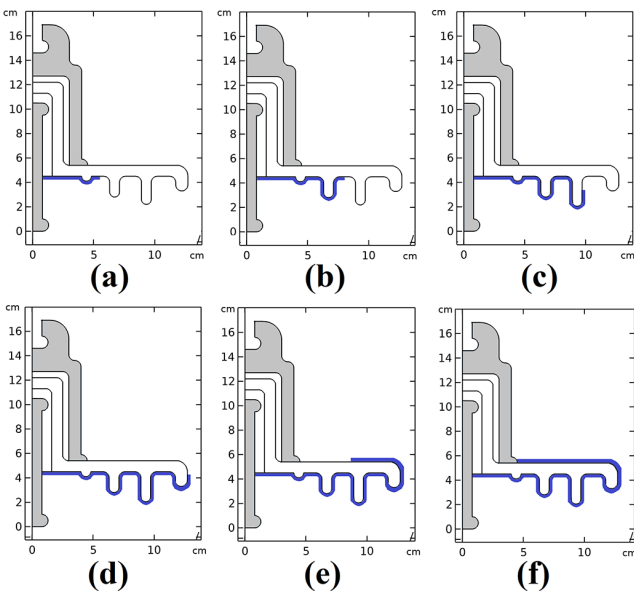
by dividing the volume of the pollution solution (V_p) by the insulator surface (S_p) [25]. The S_p of the insulator was determined using the "geometry surface measurement" property of COMSOL, and we obtained $S_p = 0.147$ m^2. The remaining volume on the insulator surface is approximately 15 ml or 1.5×10^{-5} m^3, which was measured by collecting the volume runoff from the surface during the spraying time in a container and subtracting it from the volume sprayed.

The effect of adding NaCl on the volume of the pollutant solution was neglected due to the small amount of the NaCl mass, which is very small compared to the total volume (with max of 0.25 g/L). Thereby:

$$e_p = \frac{V_p}{S_p} = \frac{1.5 \times 10^{-5}}{0.147} = 1.02 \times 10^{-4} \cong 10^{-4} \text{m}. \quad (1)$$

Researchers in [26] have found that for NaCl solution, electrical current does not flow through the entire thickness of the solution. Rather, there is an effective thickness that contributes to electrical conduction, representing a part of the total thickness. To take into account this effect in our simulation, we set the value of the pollution thickness (e_p) and measured the ratio between the simulated and experimental LC. Basing on the considerations adopted in [26] and after conducting several tests, we found that the estimated ratio of effective thickness was approximately one percent. This value was considered for the entirety of the study.

Finally, when arcing discharges are initiated, local arcs can form across the air, occurring when the local electric field exceeds the breakdown strength ($E_c = 30$ kV/cm) [27]. In the proposed simulation, this phenomenon is modelled by an effective change in air conductivity from very low $\sigma_{air} = 10^{-18}$ S/m [24] to relatively high levels. When a local arc starts to appear, the initial estimated conductivity of the air becomes $\sigma_{air} = 5 \times 10^{-2}$ S/m [28]. Fig. 5 presents the

Table 2 Material parameters of the glass insulator [24]

|	Glass	Cap and pin	Cement	Air
Relative permittivity ε_r	6	1	15	1.0005
Electric conductivity σ (S/m)	10^{-14}	10^4	10^{-6}	σ (E)

Fig. 4 Illustration of pollution layer distribution with different widths shown in blue colour: (a) 5 cm, (b) 10 cm, (c) 15 cm, (d) 20 cm, (e) 25 cm, and (f) uniform
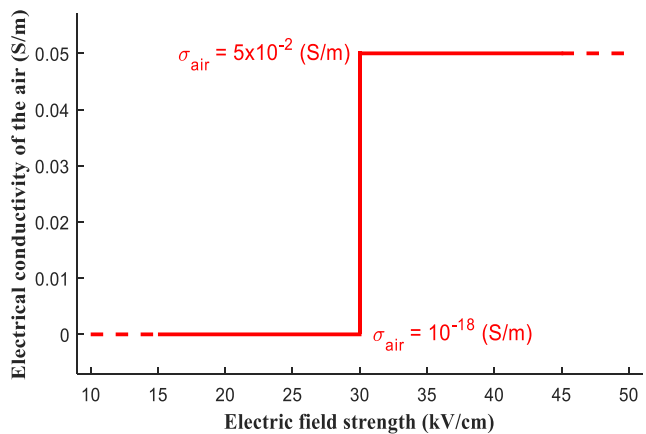

Fig. 5 Electrical conductivity of the air as a function of the electric field strength

electrical conductivity of the air as a function of the electric field σ (E). The simulation steps used to extract LC waveforms are summarized in the flowchart presented in Fig. 6.

4 Leakage current results

As the experimental setup is not protected against short-circuits, voltage levels lower than the flashover value were used to record the LC. First, we determined the flashover and arcing initiation voltages before recording LC waveforms. Tables 3 and 4 presents the experimental
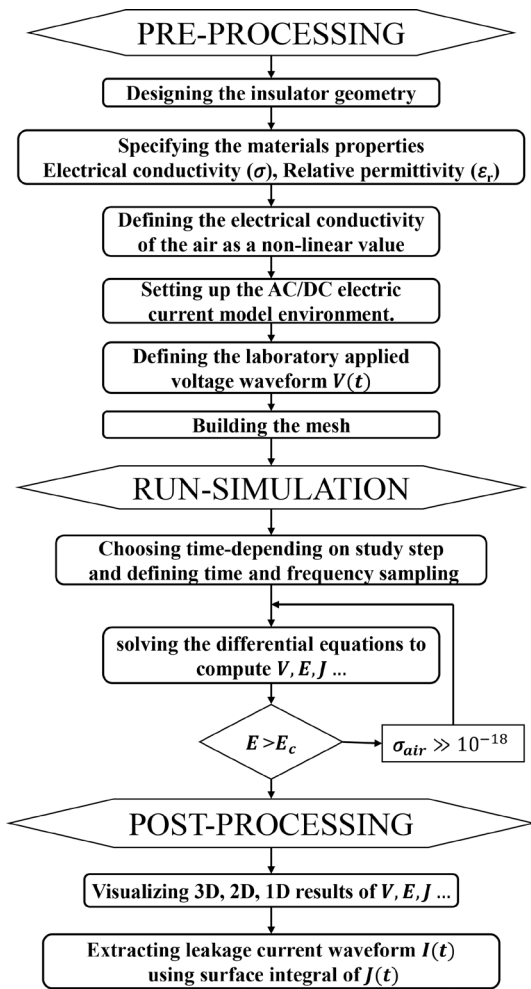

Fig. 6 Flowchart of the simulation technique

Table 3 Flashover and arcing voltages versus uniform pollution conductivity

Conductivity (µS/cm)	20	150	340
Flashover voltage (kV)	71.5	69	61
Arcing voltage (kV)	36	32	29

Table 4 Flashover and arcing voltages versus non-uniform pollution width

Pollution width (cm)	0	5	10	15	20	25
Flashover voltage (kV)	72	70	65	55	35	25
Arcing voltage (kV)	48	26	22	18	17	14

results of both voltages with respect to the uniform and non-uniform pollution conditions.

The increase in pollution conductivity or width engenders a decrease in both flashover and arcing voltages leading to the insulating system's dielectric strength decrease.

It is important to ensure that a maximum voltage of 30 kV was adopted for recording the LC waveforms for all pollution configurations, except for a non-uniform pollution width of 25 cm where the voltage was reduced to 15 kV due to flashover occurrence at 25 kV.

For further understanding of the LC behavior, we present also the current density. This latter is an important feature relating the relative permittivity and electric conductivity with the electric field to the electric current.

Measuring the potentials along the insulator surfaces, achieved through a non-contact Kelvin probe via an electrostatic voltmeter, can serve as a technique for verifying simulations. This technique demonstrated acceptable agreement between the numerical and experimental studies in the literature such as in [29]. In this research, simulation results of cap-pin glass insulator, under clean and various surface pollution conditions, is investigated utilizing the leakage current data.

4.1 Uniform pollution

LC magnitudes versus applied voltage for both experimental and simulation tests are presented in Fig. 7. On the other hand, the average relative error between the two LC recordings is illustrated in Fig. 8.

The uniform pollution layer forms a continuous film connecting the insulator electrodes, creating a path through it for the LC flows. As a result, increasing the conductivity leads to an increase in the LC magnitude. During experimental tests, several scenes were observed based on the
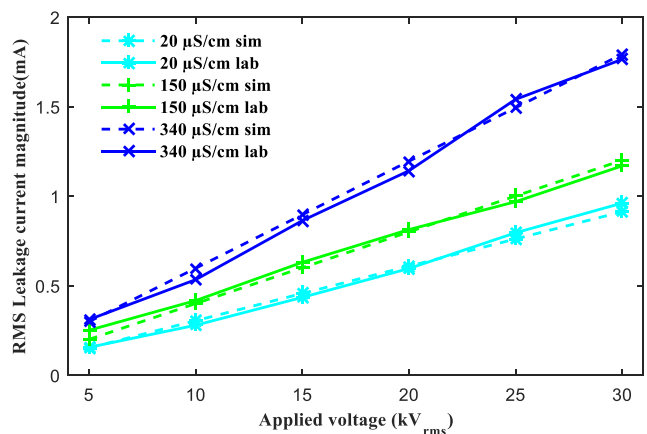

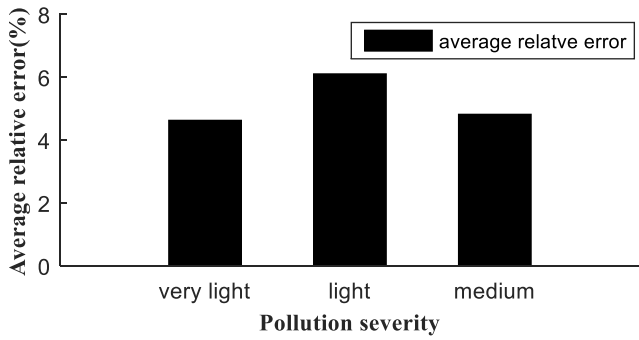**Fig. 7** LC magnitude versus applied voltage for uniform pollution conditions

Fig. 8 Average relative error versus pollution severity

uniform pollution conductivity values. For pollution conductivities not exceeding 340 µS/cm (Fig. 7), the LC magnitude increases with voltage. For this range of conductivities, the simulated LC magnitudes are practically close to those found experimentally, with an average relative error of about 4.63%, 6.11%, and 4.82% for light, very light, and medium pollution severities, respectively (Fig. 8).

In Fig. 9, the simultaneous presentation of LC waveforms evolution for different pollution conductivities from both simulation and experimental tests are shown. Fig. 9 demonstrate that the LC waveforms and their maximum values are greatly influenced by the pollution conductivity.

For light, very light, and medium pollution severities, the LC waveforms are noticeably distorted with a phase angle close to 90 degrees between the voltage and current waveforms, indicating that the capacitive behavior of the insulation system is predominant. The phase angle gradually decreases as the conductivity increases. Although there is a good similarity in waveform shape between the simulation and experimental LCs.
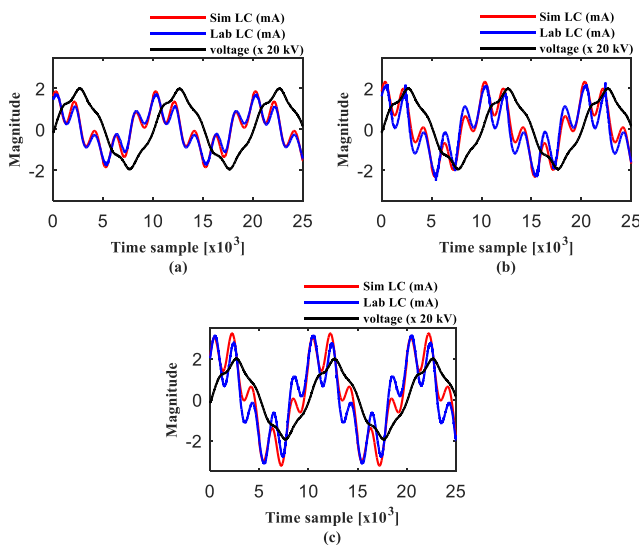

Fig. 9 LC waveforms for different pollution conductivities: (a) 20 µS/cm, (b) 150 µS/cm, (c) 340 µS/cm

As main results for uniform pollution, LC increases with voltage and pollution conductivity and the simulation results is in good agreement with experimental one for light, very light, and medium pollution severity.

4.2 Non-uniform pollution

The LC magnitudes versus pollution layer widths for both experimental and simulation tests are presented in Fig. 10 for several applied voltage levels. Fig. 10 shows the relationship between the LC magnitude and the variation of the pollution layer width at the insulator surface. It is observed that, for given pollution width, the LC magnitude increases with the applied voltage. Meanwhile, and for a given applied voltage level, the LC magnitude increases only when the pollution width is increased from 0 (the clean insulator case) to a 5 cm pollution width. Beyond this value, the LC magnitude remains almost stable; indicating that, in front of the dominance of clean zones, the enlargement of the pollution widths has practically no effect on the variation of LC.

Fig. 11 presents the average relative error between the experimental and simulation LC magnitudes. This
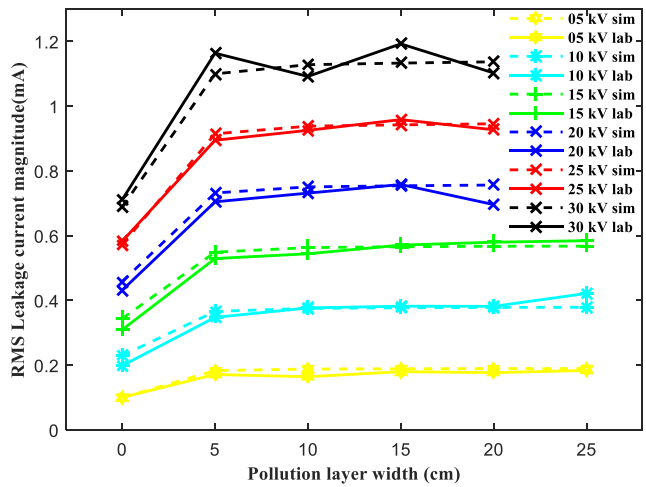

Fig. 10 LC magnitudes versus pollution layer width for different voltages
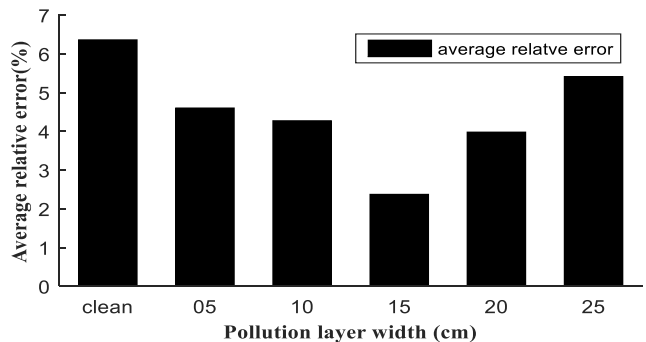

Fig. 11 Average relative error versus pollution layer widths

comparison was conducted to discuss the validity of the simulation. It is observed that the simulation results are in perfect agreement with the experimental ones obtained for clean insulator and pollution widths of 5, 10, 15, 20, and 25 cm, with average relative errors of 6.36%, 4.60%, 4.27%, 2.37%, 3.98%, and 5.41%, respectively.

The LC waveforms for the clean surface and pollution widths of 5, 10, 15, and 20 cm under a 30 kV applied voltage are presented in Fig. 12. Fig. 12 reinforces the agreement between both experimental and simulation LC waveforms. These latter exhibit distortions and an almost 90-degree shift between current and voltage due to the capacitive behavior of the dry band effect. It is noteworthy that arcing activities begin to occur for both simulation and experimental tests at relatively higher voltages (30 kV in this case). However, the shapes and magnitudes of the waveforms remain relatively the same for all pollution widths.

As the LC is closely related to current density, it is important to highlight the variation of this density as function of the pollution width. Indeed, we present in the Fig. 13 the current density streamlines versus pollution layer width.

For the clean insulator, the current density streamlines are concentrated in the radial zone delimitated by the cap and pin and constituted of cement and glass materials (in red color in Fig. 13 (a)). Meanwhile, for all pollution

layer widths, we notice that high concentration of the current density streamlines is located through the glass near the end of the cap (as shown by the red streamlines circled in Fig. 13 (b) to (f)). Indeed, in pollution conditions, the glass thickness has a more dominant impact on the current density than the surrounding air. Such finding is obvious due to the high relative permittivity of the glass to the air one.

5 Electric field results
Section 5 is devoted to the simulation of the electric field along the insulating system. We present our results for the maximum electric field value that can be reached during the application of a 30 kV voltage.

5.1 Uniform pollution
Fig. 14 illustrates simulation results of the electric field and the equipotential distributions for the considered pollution conductivities. It is noticed that both the electric field and equipotential line distributions do not change too much when the pollution conductivity increases.

The highest electric field strength is located in the HV electrode side. Meanwhile, significant electric field intensity is observed on the pollution layer near the HV electrode. The equipotential lines gradually extend from the HV to the ground electrode, with some bunches of lines taking the path through the pollution layer.

Additional details regarding the electric field distribution along the leakage path is presented in Fig. 15. As the electric conductivity of the pollution layer increases, so does the electric field. For all pollution surface conductivities, the highest value of the electric field is observed at 3 cm (from the HV terminal) on the pollution layer, with a maximum intensity of 21.1, 24.5 and 25.8 kV/cm for very
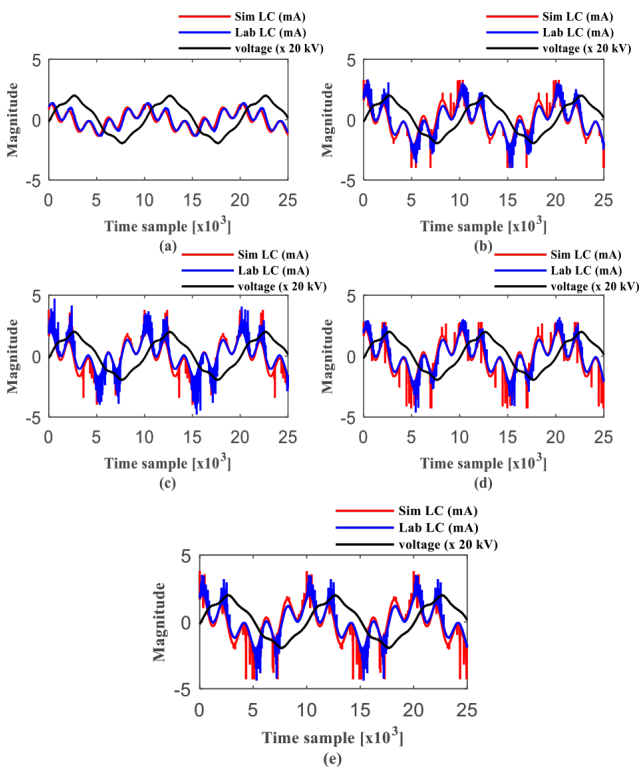

Fig. 12 LC waveforms for different pollution layer widths: (a) clean, (b) 5 cm, (c) 10 cm, (d) 15 cm, and (e) 20 cm
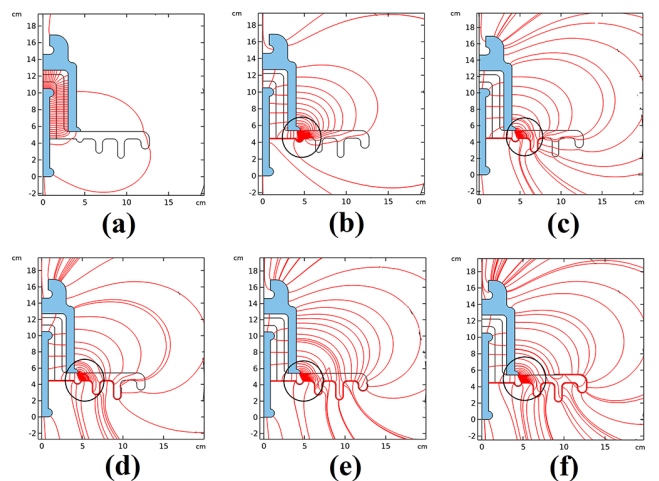

Fig. 13 Current density streamlines for different pollution layer width: (a) clean, (b) 5 cm, (c) 10 cm, (d) 15 cm, (e) 20 cm, and (f) 25 cm
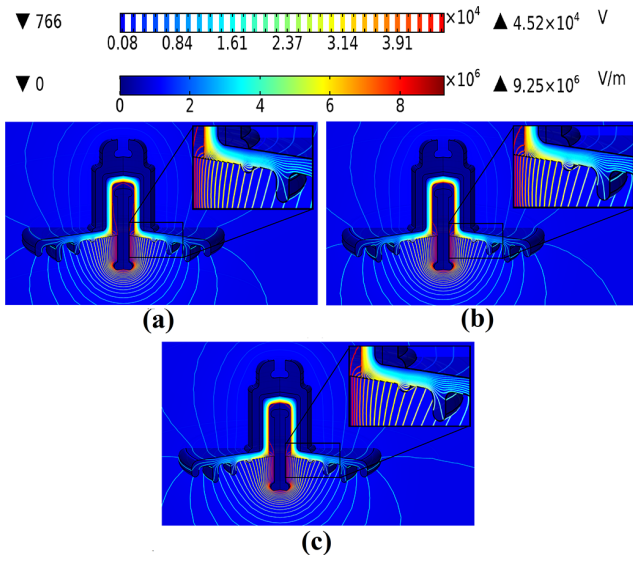
Fig. 14 Electric field and equipotential line distributions for different pollution conductivities: (a) 20 μS/cm, (b) 150 μS/cm, (c) 340 μS/cm
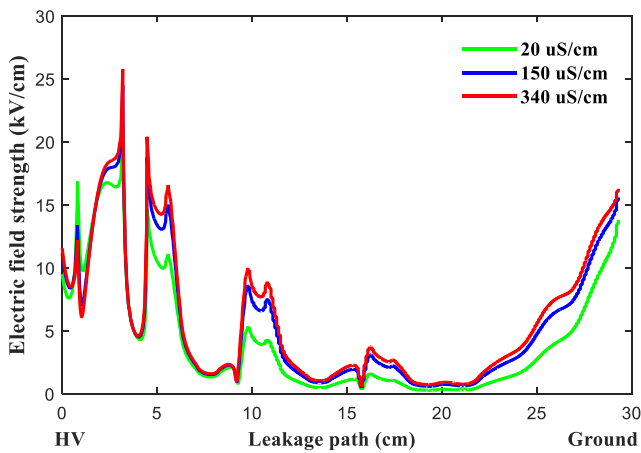

Fig. 15 Electric field distribution along the leakage path for the uniform case under a 30 kV applied voltage

Fig. 16 Electric field and equipotential lines distribution for different pollution layer width: (a) clean, (b) 5 cm, (c) 10 cm, (d) 15 cm, (e) 20 cm, and (f) 25 cm

light (20 μS/cm), light (150 μS/cm) and medium (340 μS/cm) pollution respectively. Since these values are less than the critical field of the air ionization (of 30 kV/cm), no electric discharge will occur on the insulator surface.

On the other hand, the electric field intensity is significantly reduced at the end of the ribs of the glass material, where only a small amount of charge accumulates, as mentioned in [20].

5.2 Non-uniform pollution

The impact of pollution on the electric field distribution was further studied by increasing the width of the pollution layer from the HV electrode up to 25 cm, by step of 5 cm. The results of this analysis are shown in Fig. 16, in which the clean insulator serves as a reference.
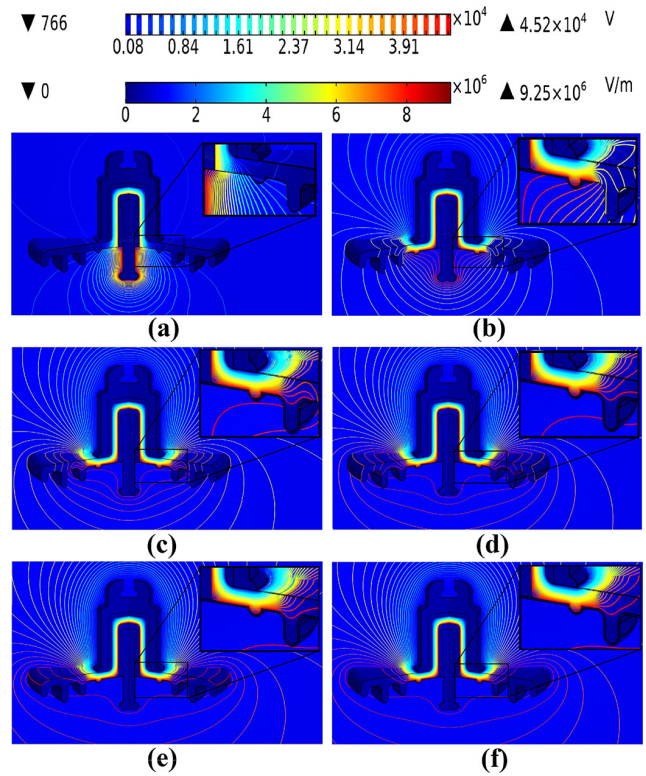
For the clean insulator surface state, the highest electric field strength was observed at the triple point constituted by the electrode, air, and dielectric near the HV side. However, for all pollution layer widths, significant electric field strength is located along the pollution at 5 cm from the HV terminal. The equipotential lines are concentrated on HV side and along the pollution layers.

The distribution of the electric field along the leakage path is illustrated in Fig. 17. It has been observed that the surface condition under non-uniform pollution affects only the distribution of the electric field, and not its maximum intensity. Indeed, for all pollution widths, the highest intensity of 46.9 kV/cm was observed at the triple region constituted by the insulator cap, air, and dielectric. The fact that this electrical field is greater than the critical value of the air ionization (of 30 kV/cm), dry band arcing are observed in this triple region as shown in Fig. 18 (a). This finding is confirmed by the high current density obtained by simulation and presented in Fig. 18 (b).

The simulation not only saves time and laboratory materials but also provides enhanced security compared to conducting certain tests in real life. As a complement to this research, we have conducted an investigation involving
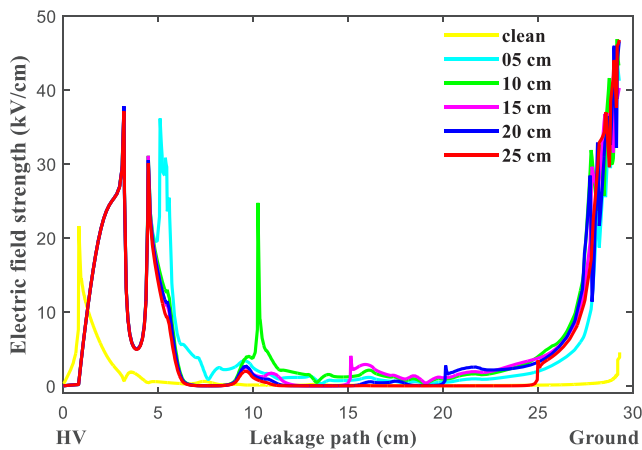
Fig. 17 Electric field distribution along the leakage path for the non-uniform case under a 30 kV applied voltage
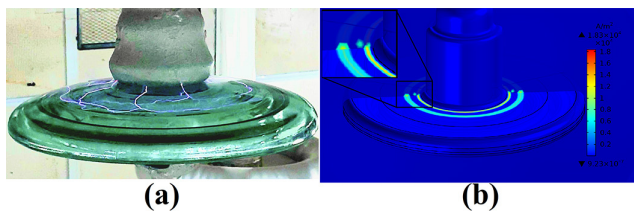

Fig. 18 Arcing discharge activity under potential of 30 kV for a pollution layer width of 15cm: (a) Experimental, (b) simulation

the same cap-pin glass insulator studied in this paper. This investigation focuses on optimizing the corona ring of the cap-pin string insulator of the 400 kV line through simulation, aiming to reduce the electric field stress along its surface by optimizing the corona ring design [30]. The results unveiled a significant reduction in the surface electric field following the implementation of optimization strategies.

6 Conclusion
This paper deals within the electrical behavior of the cap-pin insulator under uniform pollution and non-uniform pollution conditions. For the first pollution type, several conductivities are selected to represent light (20 µS/cm), very light (150 µS/cm), and medium (340 µS/cm) pollution

severities. Different widths of the pollution layer with heavy conductivity (1050 µS/cm) are considered for the second pollution type. Simulation and experimental methods have been employed for this purpose.

For both pollution conditions, the experimental LC have been recorded for applied voltage levels not exceeding 30 kV. The LC magnitudes obtained from simulation are in a good agreement with the experimental. In the uniform pollution condition case, the average relative error is about 4.63%, 6.11%, and 4.82% for light, very light, and medium pollution severities, respectively. This error is about 6.36%, 4.60%, 4.27%, 2.37%, 3.98%, and 5.41% for the pollution layer width (non-uniform pollution) of 0 (clean insulator), 5, 10, 15, 20, and 25 cm respectively.

Otherwise, the LC magnitude increases with the uniform pollution conductivity. On the other hand, the LC magnitude remains almost stable with the variation of (non-uniform) pollution width. The current density distribution analysis offers valuable interpretation into this finding, indicating a high concentration of current density through the glass located near the end of the cap.

The maximum electric field of 25.8 kV/cm was observed and located at a distance of 3 cm from the HV terminal on the uniform pollution layer. On the other hand, the maximum electric field of 46.9 kV/cm was observed at the triple region constituted by the insulator cap, air, and dielectric. Since this electric field (46.9 kV/cm) exceeds the critical field of air ionization (30 kV/cm), arcing discharges occur in the triple region. Such discharges have been observed during both experiments and simulation (in term of high current density concentration).

Comparing simulations with experimental data for a given set of electrical characteristics, such as leakage current, helps not only with the verification of the results but also with paving the way for providing further clarification and understanding of the results as well as opening new research aspects such as optimization applications.

References
[1] Bojovschi, A., Quoc, T. V., Trung, H. N., Quang, D. T., Le, T. C. "Environmental Effects on HV Dielectric Materials and Related Sensing Technologies", Applied Sciences, 9(5), 856, 2019. https://doi.org/10.3390/app9050856
[2] Ntuli, M., Mbuli, N., Motsoeneng, L., Xezile, R., Pretorius, J. H. C. "Increasing the capacity of transmission lines via current uprating: An updated review of benefits, considerations and developments", In: 2016 Australasian Universities Power Engineering Conference (AUPEC), Brisbane, QLD, Australia, 2016, pp. 1–6. ISBN 978-1-5090-1406-4 https://doi.org/10.1109/AUPEC.2016.7749338
[3] Gouda, O. E., Darwish, M. M. F., Mahmoud, K., Lehtonen, M., Elkhodragy, T. M. "Pollution Severity Monitoring of High Voltage Transmission Line Insulators Using Wireless Device Based on Leakage Current Bursts", IEEE Access, 10, pp. 53713–53723, 2022. https://doi.org/10.1109/ACCESS.2022.3175515
[4] George, J.-M., Ferreira, L. F. "HVDC Overhead Line Insulators Selection and Design Update Features", In: 2018 XXXI International Summer Meeting on Power and Industrial Applications (RVP-AI), Acapulco, Mexico, 2018, pp. 126–130. ISBN 978-1-5386-7454-3 https://doi.org/10.1109/RVPAI.2018.8469831

[5] George, J.-M., Prat, S., Lumb, C., Virlogeux, F., Gutman, I., Lundengard, J., Marzinotto, M. "Field experience and laboratory investigation of glass insulators having a factory-applied silicone rubber coating", IEEE Transactions on Dielectrics and Electrical Insulation, 21(6), pp. 2594–2601, 2014.
https://doi.org/10.1109/TDEI.2014.004600

[6] Ramesh, R., Sugumaran, C. P. "Reduction of flashover in ceramic insulator with nanocomposites", In: 2017 3rd International Conference on Condition Assessment Techniques in Electrical Systems (CATCON), Rupnagar, India, 2017, pp. 418–422. ISBN 978-1-5386-3139-3
https://doi.org/10.1109/CATCON.2017.8280256

[7] Ghermoul, O., Benguesmia, H., Benyettou, L. "Finite element modeling for electric field and voltage distribution along the cap and pin insulators under pollution", Diagnostyka, 24(2), 2023201, 2023.
https://doi.org/10.29354/diag/159517

[8] Zhang, Z., Liu, X., Jiang, X., Hu, J., Gao, D. W. "Study on AC Flashover Performance for Different Types of Porcelain and Glass Insulators With Non-Uniform Pollution", IEEE Transactions on Power Delivery, 28(3), pp. 1691–1698, 2013.
https://doi.org/10.1109/TPWRD.2013.2245153

[9] Maadjoudj, D., Kherif, O., Mekhaldi, A., Teguar, M. "Features Characterizing the Surface State of HV Insulator Glass Model under Desert Pollution", IEEE Transactions on Dielectrics and Electrical Insulation, 28(6), pp. 1964–1972, 2021.
https://doi.org/10.1109/TDEI.2021.009739

[10] Sadykova, D., Pernebayeva, D., Bagheri, M., James, A. "IN-YOLO: Real-Time Detection of Outdoor High Voltage Insulators Using UAV Imaging", IEEE Transactions on Power Delivery, 35(3), pp. 1599–1601, 2020.
https://doi.org/10.1109/TPWRD.2019.2944741

[11] Salem, A. A., Abd-Rahman, R., Al-Gailani, S. A., Kamarudin, M. S., Ahmad, H., Salam, Z. "The Leakage Current Components as a Diagnostic Tool to Estimate Contamination Level on High Voltage Insulators", IEEE Access, 8, pp. 92514–92528, 2020.
https://doi.org/10.1109/ACCESS.2020.2993630

[12] Villalobos, R. J., Moran, L. A., Huenupán, F., Vallejos, F., Moncada, R., Pesce, C. G. "A New Current Transducer for On-Line Monitoring of Leakage Current on HV Insulator Strings", IEEE Access, 10, pp. 78818–78826, 2022.
https://doi.org/10.1109/ACCESS.2022.3191349

[13] Abeysekara, A. H. A. D., Kumara, J. R. S. S., Fernando, M. A. R. M., Eakanayake, M. P. B., Godaliyadda, G. M. R. I., Wijayakulasooriya, J. V. "Remote leakage current detector for identification of insulators discharges", IEEE Transactions on Dielectrics and Electrical Insulation, 24(4), pp. 2449–2458, 2017.
https://doi.org/10.1109/TDEI.2017.006300

[14] Roman, M., van Zyl, R. R., Parus, N., Mahatho, N. "In-Situ Monitoring of Leakage Current on Composite and Glass Insulators of the Cahora Bassa HVDC Transmission Line", SAIEE Africa Research Journal, 110(1), pp. 4–10, 2019.
https://doi.org/10.23919/SAIEE.2019.8643145

[15] Sartika, N., Naufalarizqa, R. M. P., Rachmawati, Suwarno. "Study on leakage current characteristics and computer simulation of semiconducting glazed insulator under clean and salt fog condition", In: 2018 12th International Conference on the Properties and Applications of Dielectric Materials (ICPADM), Xi'an, China, 2018, pp. 82–85. ISBN 978-1-5386-5789-8
https://doi.org/10.1109/ICPADM.2018.8401082

[16] Palangar, M. F., Mirzaie, M., Mahmoudi, A. "Improved flashover mathematical model of polluted insulators: A dynamic analysis of the electric arc parameters", Electric Power Systems Research, 179, 106083, 2020.
https://doi.org/10.1016/j.epsr.2019.106083

[17] Doufene, D., Bouazabia, S., Ladjici, A. A. "Shape optimization of a cap and pin insulator in pollution condition using particle swarm and neural network", In: 2017 5th International Conference on Electrical Engineering - Boumerdes (ICEE-B), Boumerdes, Algeria, 2017, pp. 1–4. ISBN 978-1-5386-0687-2
https://doi.org/10.1109/ICEE-B.2017.8192094

[18] M'hamdi, B., Teguar, M., Mekhaldi, A. "Optimal design of corona ring on HV composite insulator using PSO approach with dynamic population size", IEEE Transactions on Dielectrics and Electrical Insulation, 23(2), pp. 1048–1057, 2016.
https://doi.org/10.1109/TDEI.2015.005383

[19] Abimouloud, A., Arif, S., Korichi, D., Ale-Emran, S. M. "Prediction of DC flashover voltage of cap-and-pin polluted insulator", IET Science, Measurement & Technology, 13(2), pp. 279–286, 2019.
https://doi.org/10.1049/iet-smt.2018.5105

[20] Salem, A. A., Abd-Rahman, R., Rahiman, W., Al-Gailani, S. A., Al-Ameri, S. M., Ishak, M. T., Sheikh, U. U. "Pollution Flashover Under Different Contamination Profiles on High Voltage Insulator: Numerical and Experiment Investigation", IEEE Access, 9, pp. 37800–37812, 2021.
https://doi.org/10.1109/ACCESS.2021.3063201

[21] Thomas, A. J., Iyappan, C., Reddy, C. C. "On the Measurement of Surface Voltage of Insulators and Bushings", IEEE Transactions on Power Delivery, 37(1), pp. 464–471, 2022.
https://doi.org/10.1109/TPWRD.2021.3063346

[22] IEC "IEC TS 60815-1:2008 Selection and dimensioning of high-voltage insulators intended for use in polluted conditions - Part 1: Definitions, information and general principles", International Electrotechnical Commission, Geneva, Switzerland, 2008.

[23] IEC "IEC 60507:2013 Artificial pollution tests on high-voltage ceramic and glass insulators to be used on a.c. systems", Geneva, Switzerland, 2013.

[24] Salhi, R., Mekhaldi, A., Teguar, M., Kherif, O., Slama, M. E. A. "Cap-Pin Glass Insulator Simulation and Leakage Current waveform Extraction", In: 2022 2nd International Conference on Advanced Electrical Engineering (ICAEE), Constantine, Algeria, 2022, pp. 1–4. ISBN 978-1-6654-1742-6
https://doi.org/10.1109/ICAEE53772.2022.9961979

[25] Araya, J., Montaña, J., Schurch, R. "Electric Field Distribution and Leakage Currents in Glass Insulator Under Different Altitudes and Pollutions Conditions using FEM Simulations", IEEE Latin America Transactions, 19(8), pp. 1278–1285, 2021.
https://doi.org/10.1109/TLA.2021.9475858

[26] Slama, M. E. A., Beroual, A., Hadi, H. "Influence of the linear non-uniformity of pollution layer on the insulator flashover under impulse voltage - estimation of the effective pollution thickness", IEEE Transactions on Dielectrics and Electrical Insulation, 18(2), pp. 384–392, 2011.
https://doi.org/10.1109/TDEI.2011.5739441

[27] Diesendorf, W. "Insulation Co-ordination in High Voltage Electric Power Systems", Butterworth-Heinemann, 1974. ISBN 978-0-408-70464-9
https://doi.org/10.1016/C2013-0-01020-1

[28] Farzaneh, M., Fofana, I. "Study of Insulator Flashovers caused by Atmospheric Ice Accumulation", Journal of Iranian Association of Electrical and Electronics Engineers, 1(1), pp. 10–23, 2004. [online] Available at: https://sid.ir/paper/551086/en [Accessed: 23 July 2023]

[29] Ilhan, S., Ozdemir, A., Jayaram, S. H., Cherney, E. A. "Numerical and experimental investigation of the effects of pollution on glass suspension-type insulators", IEEE Transactions on Dielectrics and Electrical Insulation, 22(5), pp. 2987–2994, 2015.
https://doi.org/10.1109/TDEI.2015.004863

[30] Salhi, R., Mekhaldi, A., Teguar, M., Kherif, O. "Optimizing Corona Ring Design for 400 kV Cap-Pin String Insulator to Minimize Surface Electric Field under Various Surface Conditions", In: 2023 International Conference on Electrical Engineering and Advanced Technology (ICEEAT), Batna, Algeria, 2023, pp. 1–5. ISBN 979-8-3503-8349-2
https://doi.org/10.1109/ICEEAT60471.2023.10426163